Rabenosyn-5 defines the fate of the transferrin receptor following clathrin-mediated endocytosis

Deanna M. Navaroli[a,1], Karl D. Bellvé[b,1], Clive Standley[b,1], Lawrence M. Lifshitz[b], James Cardia[c], David Lambright[a], Deborah Leonard[a], Kevin E. Fogarty[b], and Silvia Corvera[a,2]

[a]Program in Molecular Medicine and [b]Biomedical Imaging Group, University of Massachusetts Medical School, Worcester MA 01605; and [c]RXi Pharmaceuticals Corporation, Worcester, MA 01605

Edited by Jennifer Lippincott-Schwartz, National Institutes of Health, Bethesda, MD, and approved December 20, 2011 (received for review September 21, 2011)

Cell surface receptors and other proteins internalize through diverse mechanisms at the plasma membrane and are sorted to different destinations. Different subpopulations of early endosomes have been described, raising the question of whether different internalization mechanisms deliver cargo into different subsets of early endosomes. To address this fundamental question, we developed a microscopy platform to detect the precise position of endosomes relative to the plasma membrane during the uptake of ligands. Axial resolution is maximized by concurrently applied total internal reflection fluorescence and epifluorescence-structured light. We found that transferrin receptors are delivered selectively from clathrin-coated pits on the plasma membrane into a specific subpopulation of endosomes enriched in the multivalent Rab GTPase and phosphoinositide-binding protein Rabenosyn-5. Depletion of Rabenosyn-5, but not of other early endosomal proteins such as early endosome antigen 1, resulted in impaired transferrin uptake and lysosomal degradation of transferrin receptors. These studies reveal a critical role for Rabenosyn-5 in determining the fate of transferrin receptors internalized by clathrin-mediated endocytosis and, more broadly, a mechanism whereby the delivery of cargo from the plasma membrane into specific early endosome subpopulations is required for its appropriate intracellular traffic.

endosomal sorting | lysosomal degradation | super resolution | receptor trafficking | patterned illumination

The endocytic pathway is known principally for its role in the uptake of receptors and ligands (1–4) and increasingly is being recognized as critical in other aspects of cell physiology. For example, the control of cellular growth through mammalian target of rapamycin signaling involves associations with late endosomal membranes (5, 6), and microRNA regulatory mechanisms are associated with endosomal/lysosomal membranes (7–9). Thus, it is necessary to understand how the distinct membrane compartments of the endocytic pathway form, traffic internalized ligands, and serve as scaffolds for the assembly of regulatory complexes.

In the classical view of the endocytic pathway (3, 10–13), internalizing cargoes are incorporated into vesicles formed by clathrin-mediated or other mechanisms of endocytosis at the plasma membrane. These vesicles fuse with a homogenous population of early endosomes from which cargo then is sorted to different destinations. However, recent results demonstrate that genetic networks involved in the early trafficking of the transferrin (Tf) and EGF receptors (TfR and EGFR, respectively) differ from each other substantially (14) and find that EGF and Tf populate different subsets of vesicles almost immediately after addition to live cells at physiological temperature (15). Further evidence for early endosome heterogeneity is found in studies in which endosomes display different motilities and different phosphoinositide effector complements (16–18). These results suggest that different populations of early endosomes exist, raising the possibility that different ligands may be directed specifically from the plasma membrane into particular early endosome classes rather than internalizing into a common early endosome.

The TfR has been studied extensively to define mechanisms involved in receptor-mediated endocytosis (3, 19). This receptor concentrates in clathrin-coated membrane regions (20), from which it enters the endosomal system. Iron bound to Tf is released at the low pH of the endosomes, and the TfR recycles to the plasma membrane and releases iron-free Tf. To visualize directly the movement of TfRs from clathrin-coated membrane structures into specific early endosome subpopulations, we developed a microscopy platform capable of simultaneously detecting three different fluorophores using total internal reflection fluorescence (TIRF). Because TIRF images confound intrinsic fluorescence brightness with axial position, the true position of an endosome relative to the plasma membrane can be obtained only if its actual brightness is known. Thus, we concurrently determined the in-focus brightness of the endosomes in the TIRF field using epifluorescence-structured light (ESL) (21, 22). The combination of TIRF and ESL microscopy (TESM) provides the precise localization of endosomes relative to the cell surface.

Among key endosomal components implicated in early endosome fusion are proteins such as early endosome antigen (1EEA1) (23, 24), adaptor protein, phosphotyrosine interaction (APPL1) (25), and Rabenosyn-5 (26). Their function is controlled by small GTPases, such as Rab4 and Rab5, and lipids such as phosphatidylinositol 3-phosphate (27–29). To determine the role of endosomes containing these proteins, we imaged each one simultaneously with clathrin and Tf. We found distinct endosome subpopulations enriched in these markers residing at different regions within the TIRF zone. Tf is internalized from clathrin-coated regions at the plasma membrane into endosomes containing Rabenosyn-5. Depletion of Rabenosyn-5, but not of EEA1, results in TfR missorting and extensive degradation, coupled with alterations in clathrin dynamics. These results reveal the importance of Rabenosyn-5 in early endosomal trafficking of cargo internalized through clathrin-mediated mechanisms and suggest that specific endosome populations are involved in the trafficking of cargo entering through distinct plasma membrane internalization pathways.

Results

Flux of Tf from the Plasma Membrane Through the Endosomal System. To visualize the movement of Tf from clathrin-enriched plasma membrane regions into the endosomal system, Tf-DyLight-649

Author contributions: D.M.N., K.D.B., C.S., L.M.L., D. Lambright, D. Leonard, K.E.F., and S.C. designed research; D.M.N. and D. Leonard performed research; K.D.B., L.M.L., J.C., D. Lambright, and D. Leonard contributed new reagents/analytic tools; D.M.N., L.M.L., D. Lambright, D. Leonard, K.E.F., and S.C. analyzed data; and K.E.F. and S.C. wrote the paper.

The authors declare no conflict of interest.

This article is a PNAS Direct Submission.

[1]D.M.N., K.D.B., and C.S. contributed equally to this work.

[2]To whom correspondence should be addressed. E-mail: silvia.corvera@umassmed.edu.

See Author Summary on page 2702 (volume 109, number 8).

This article contains supporting information online at www.pnas.org/lookup/suppl/doi:10.1073/pnas.1115495109/-/DCSupplemental.

was added to cells cotransfected with TagRFP-T-clathrin and EGFP-tagged Rabenosyn-5, APPL1, or EEA1. Cells were imaged at 1 Hz (one frame/s) continuously for 15 min: 5 min before the addition, 5 min in the presence, and 5 min after the removal of Tf-DyLight-649. Fig. 1*A* illustrates one time frame of the resulting 900-image set, taken 1 min after the addition of Tf, and Movie S1 illustrates the image set. To analyze these complex time-lapse image sets systematically, we used the method illustrated in Fig. 1*B* and further described in *Materials and Methods*. This method identifies all individual structures within the image and measures the relative amount of Tf specifically associated with them at each time point. In this example, images of TagRFP-T-clathrin (Fig. 1*B*, *Top*, Unprocessed) are first convolved using a difference of Gaussians (DOG) filter to eliminate the diffuse signal originating from out-of-focus or auto fluorescence (Fig. 1*B*, *Top*, DOG). The pixel of highest intensity within each region is identified (Fig. 1*B*, *Top*, MIP) and is mapped on the unprocessed clathrin image (Fig. 1*B*, *Middle Left*). A 5 × 5 pixel square (25 pixels) surrounding this pixel is outlined (Fig. 1*B*, *Middle Right*), and its mean intensity [clathrin (in)] is recorded. From this value, the mean intensity of a one-pixel-wide frame (24 pixels) surrounding the square (Fig. 1*B*, *Middle Right*, hatched regions) is subtracted [clathrin (out)], thus subtracting the local background. The positions of the maximum-intensity pixels (MIPs) derived from the clathrin image are mapped onto the corresponding unprocessed Tf image (Fig. 1*B*, *Bottom*), and the same calculation is performed. Thus, Tf has a positive value only if the signal detected within the 5 × 5 pixel region is higher than that of the immediate surrounding region. The ratio of the values obtained [Tf (in) − Tf (out)/clathrin (in) − clathrin (out)] for each region then is calculated, and the mean of all regions in the image is plotted for each time point (Fig. 1*C*). In the same cell, the trafficking of Tf into Rabenosyn-5–containing endosomes is measured similarly. The data (Fig. 1*C*) are fit into a kinetic model, described in detail in the *SI Appendix*, "Curve Fits to Ratio Data" section, that incorporates known constants for Tf binding to the TfR, the concentration of free ligand, and the amount of Tf associated with clathrin.

Tf associates rapidly and saturably with clathrin-containing regions, displaying kinetic constants consistent with binding to the TfR (*SI Appendix*, Table S1) (30–32). Interestingly, Tf is detected almost immediately within Rabenosyn-5–enriched regions, with virtually no time elapsing between the detection of Tf in clathrin-coated regions and its detection in Rabenosyn-5 endosomes, and

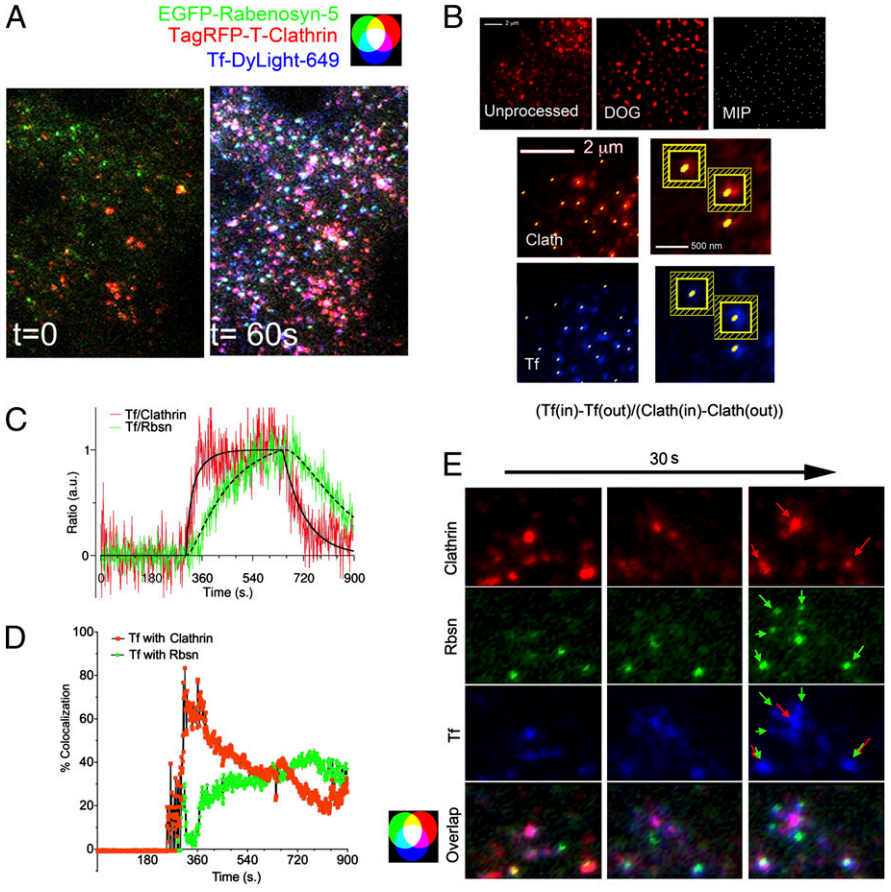

Fig. 1. Dynamics of Tf flux into Rabenosyn-5–enriched endosomes. (*A*) Cells coexpressing EGFP-Rabenosyn-5 (green) and TagRFP-T-clathrin (red) were exposed to Tf-DyLight-649 (blue). Shown are representative frames of images taken immediately before (t = 0) and 60 s after addition of Tf (t = 60 s). (*B*) A representative unprocessed image (*Top Left*) of TagRFP-T-clathrin was smoothed using a DOG filter as described in *Materials and Methods* (DOG, *Top center*), and the MIP of each region was identified (*Top Right*) and mapped onto the unprocessed clathrin (Clath, *Middle Left*) and Tf (*Bottom Left*) images. Areas of 5 × 5 pixels (in) and a surrounding one-pixel-wide frame (out) were delineated around each MIP in each image (*Middle Right* and *Bottom Right*). **(***C*) The average ratio of [Tf(in) − Tf (out)]/[Clath(in) − Clath(out)] and [Tf(in) − Tf (out)]/[Rbsn(in) − Rbsn(out)] of all MIPs at each time point was calculated and normalized to a maximum of 1. (*D*) Percent of Tf pixels colocalized with clathrin (red) or Rabenosyn-5 (green) over time. Spikes seen upon addition and removal of Tf are caused by temporary focus shifts, which recover rapidly. This experiment was repeated four times with similar results (*SI Appendix*, Table S1). (*E*) Representative images showing Tf associating with clathrin-enriched regions (red arrows) and subsequently with Rabenosyn-5 endosomes (green arrows). Rbsn, Rabenosyn-5; Clath, clathrin heavy chain.

continues to accumulate in these endosomes as long as free Tf is present. When Tf is removed from the medium, it disappears rapidly from clathrin-enriched regions because of transfer into the endosomal pathway (*SI Appendix*, Table S1). Strikingly, the rate of exit of Tf from clathrin-containing membrane regions (0.0053 ± 0.002/s, mean ± SEM, $n = 4$), is indistinguishable from its rate of entry into Rabenosyn-5–enriched endosomes (0.0037 ± 0.002/s, mean ± SEM, $n = 4$) (*SI Appendix*, Table S1), implying that Tf internalized via clathrin-coated pits could be delivered almost directly into Rabenosyn-5–containing endosomes.

We then calculated the net amount of Tf colocalizing with clathrin and Rabenosyn-5 over time (Fig. 1*D*). Approximately 70–80% of Tf colocalized with clathrin within 2 min of exposure and then decreased because of increasing accumulation in endosomes. The amount of Tf colocalizing with Rabenosyn-5 increased in parallel, reaching ~40% of the signal, such that >80% of Tf can be accounted for as colocalizing with either clathrin or Rabenosyn-5 4–5 min after addition. Thus, both the kinetics (Fig. 1*C*) and the net amount measured (Fig. 1*D*) indicate that the majority of Tf proceeds from clathrin-coated pits/vesicles into Rabenosyn-5–containing endosomes. Visual inspection of the images reveals numerous events consistent with this model, where Tf is seen moving from clathrin-enriched regions of the plasma membrane into endosomes containing Rabenosyn-5 localized in the immediate vicinity (Fig. 1*E*).

If indeed Tf can be delivered preferentially and rapidly to Rabenosyn-5–enriched endosomes, there may be a high degree of proximity between clathrin-coated plasma membrane regions and Rabenosyn-5–containing endosomes. TIRF imaging alone cannot be used to determine the positional relationship between these structures, because the brightness of an object can result from either its size or its distance from the cell surface (coverslip). Thus, to determine the topological relationship between clathrin-coated regions and endosomes, we concurrently obtained ESL images, which provide the actual intensity of fluorescent structures within the field. TIRF (Fig. 2*A*, TIRF) and ESL (Fig. 2*A*, ESL) images of GFP-clathrin and endogenous Rabenosyn-5 were obtained and were used to derive high-resolution 3D maps (TESM) of the position of endosomes relative to the cell surface, as described in detail in *Materials and Methods*. In these images, objects closest to the plasma membrane are displayed as blue, and those furthest away from the plasma membrane are displayed in red. Numerous endosomes containing Rabenosyn-5 are as proximal as clathrin-enriched regions to the cell surface. Similar information was obtained when clathrin and Rabenosyn were compared directly in overlapped TIRF and ESL images displayed in XZ orientation. Bright objects visible in ESL often are less visible in TIRF because of their distance from the cell surface, and objects highly visible in TIRF actually may be dimmer objects that are very close to the cell surface. These images demonstrate that Rabenosyn-5–enriched endosomes are in close proximity to clathrin-enriched regions at the cell surface, indicating that the topological organization of this pathway could accommodate a transfer from clathrin-coated pits/vesicles into these endosomes.

To determine whether the delivery of Tf into Rabenosyn-5–containing endosomes is specific, we analyzed the relationship between Tf internalization and other endosome classes. Recently it has been shown that in cells expressing the constitutively active V12G mutant of H-Ras, clathrin-mediated endocytosis gives rise to a set of endosomal intermediates containing the protein APPL1 (18). As others have reported previously (18, 25), we found APPL1 on small vesicles at the periphery of the cell image,

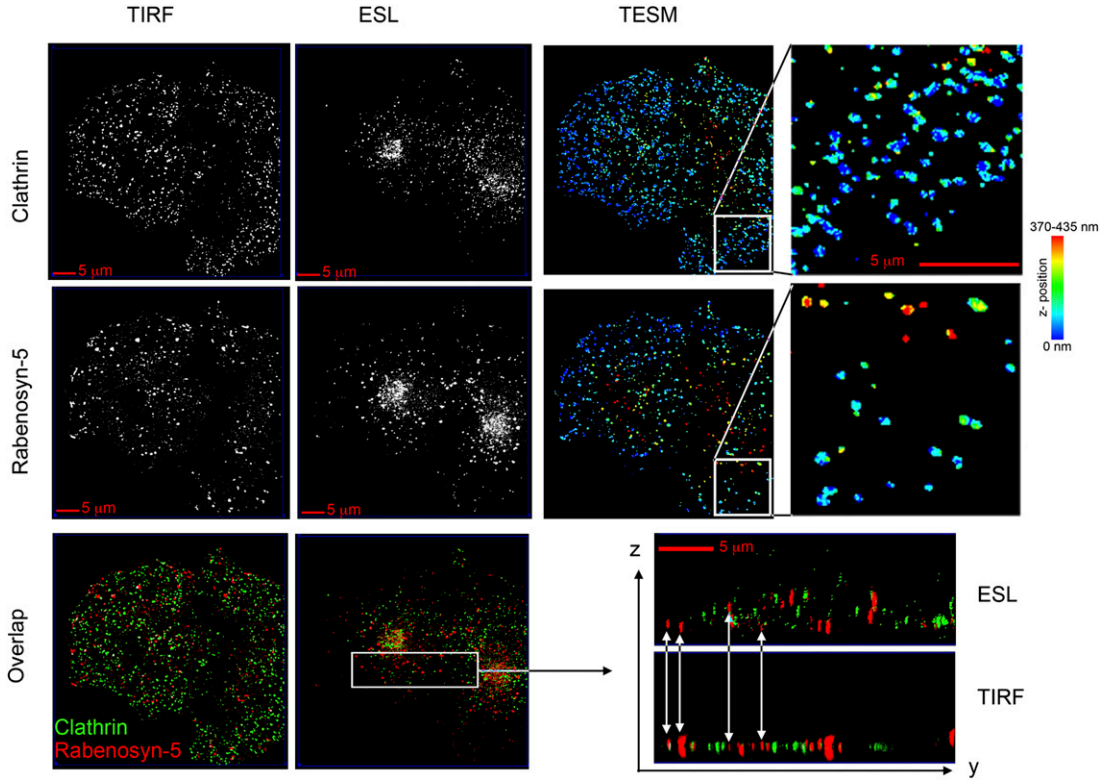

Fig. 2. Localization of Rabenosyn-5–enriched endosomes and clathrin relative to the cell surface. A COS-7 cell expressing EGFP-clathrin and stained with antibodies to endogenous Rabenosyn-5 was imaged with TIRF and ESL, and the resulting z-maps were derived by TESM. Rightmost panels are enlargements of the section indicated in panels immediately to their left. Bottom panels show overlapped images of clathrin (green) and Rabenosyn-5 (red) displayed in XY orientation and YZ orientation of the section indicated. Arrows indicate the differing depths within the cell at which the Rabenosyn-5–containing endosomes detected in the TIRF zone are found.

whereas clathrin-enriched regions are present throughout (Fig. 3*A*, *Upper*). Several of the APPL1-containing structures localize close to clathrin (Fig. 3*A*, *Lower*), consistent with the hypothesis (18) that APPL1-containing endosomes are derived from clathrin-coated vesicles. Tf occupied APPL1-containing structures at a rate similar to the rate at which it entered Rabenosyn-5 endosomes (Fig. 3*B* and *SI Appendix*, Table S2), but the net amount of Tf localizing to APPL1-enriched endosomes was almost negligible (Fig. 3*C*). In addition, only APPL1 endosomes closest to clathrin colocalized with Tf (Fig. 3*D*, overlap, white pixels), and these endosomes also contained Rabenosyn-5, as visualized in cells coexpressing EGFP-APPL1 and TagRFP-T-Rabenosyn-5 (Fig. 3*E*). Thus, Tf does not internalize through endosomes containing only APPL1.

Functional Role of Rabenosyn-5 in TfR Internalization. To examine the function of Rabenosyn-5 in Tf trafficking, we analyzed the effects of siRNA-mediated depletion. Rabenosyn-5 protein decreased 48 h after transfection and was undetectable after 72 h (Fig. 4*A*, *Top*). Surprisingly, TfR levels were decreased markedly in response to Rabenosyn-5 knockdown, with the decline beginning 48 h after transfection (Fig. 4*A*, *Middle*). This effect was specific to the TfR, because GAPDH (Fig. 4 *A* and *B*), or other elements of the endocytic pathway, such as clathrin, EEA1, and APPL1, and other receptors, such as the EGFR, were not affected (Fig. 4*B*). To determine whether other components of the early endocytic pathway would lead to similar changes in TfR levels, we compared the effects of Rabenosyn-5 and EEA1 depletion. Depletion of EEA1 did not result in TfR degradation; instead, a small but detectable increase in TfR levels was observed (Fig. 4*C*). These results demonstrate that Rabenosyn-5 and EEA1 have fundamentally different roles in Tf trafficking and are consistent with a previously proposed role of EEA1 in trafficking toward the lysosomal pathway (15). To determine whether Rabenosyn-5 depletion would, in addition to decreasing total levels, affect the cellular distribution of the TfR, we performed immunofluorescence analysis. A marked decrease in endogenous TfR levels was visible in the TIRF zone (Fig. 4*D*,

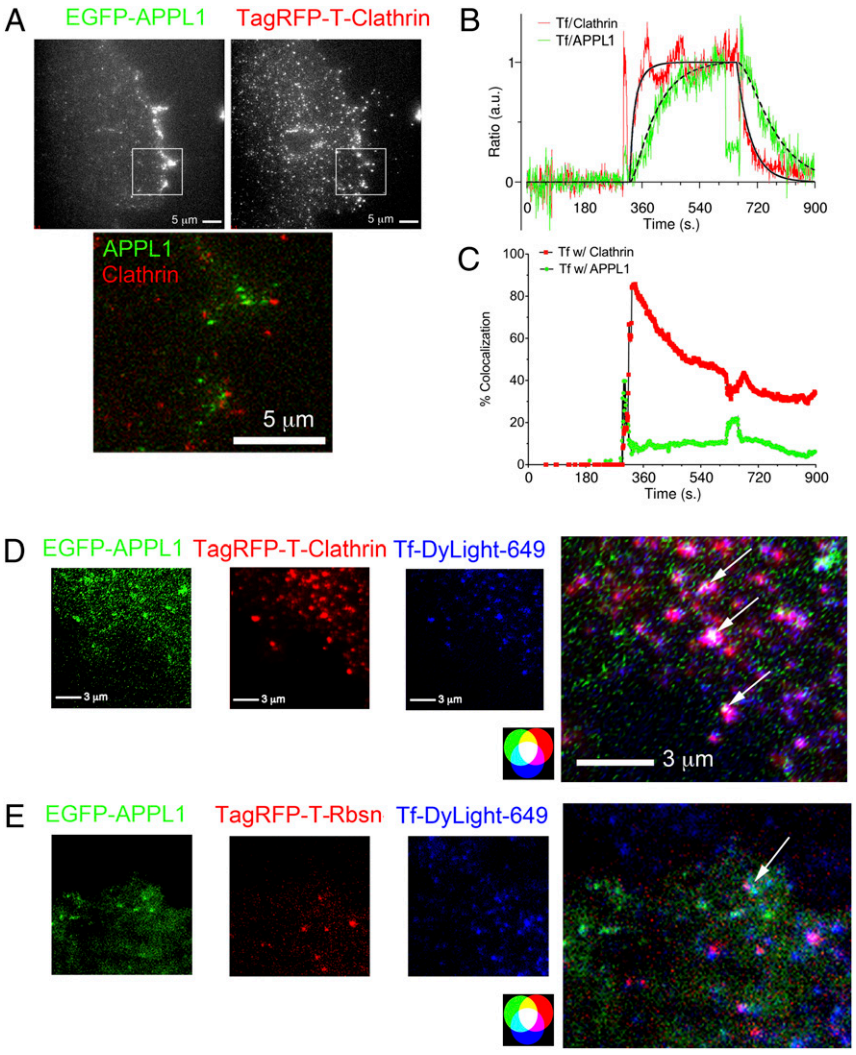

Fig. 3. Tf flux into APPL1-enriched endosomes. (*A*) Epifluorescence images of COS-7 cells coexpressing EGFP-APPL1 (green) and TagRFP-T-clathrin (red). Region of the cell showing APPL1 localizing to small vesicles at the cell periphery in proximity to clathrin. (*B*) Quantification of the ratio of [Tf(in) – Tf (out)]/[Clath(in) – Clath(out)] and [Tf(in) – Tf (out)]/[APPL(in) – APPL(out)] plotted as the mean of all regions at each time point over time. Spikes seen upon the addition and removal of Tf are caused by temporary focus shifts, which recover rapidly. (*C*) Quantification of Tf colocalization with clathrin (red) or APPL1 (green) over time; $n = 3$. (*D*) Representative image at 5 min following addition of Tf. Arrows in the overlapped image indicate the areas where clathrin, APPL1, and Tf colocalize. (*E*) Representative image of a COS-7 cell coexpressing EGFP-APPL1 and TagRFP-T-Rabenosyn-5 5 min after the addition of Tf. The arrow in the overlapped image indicates the area where APPL1, Rbsn, and Tf colocalize.

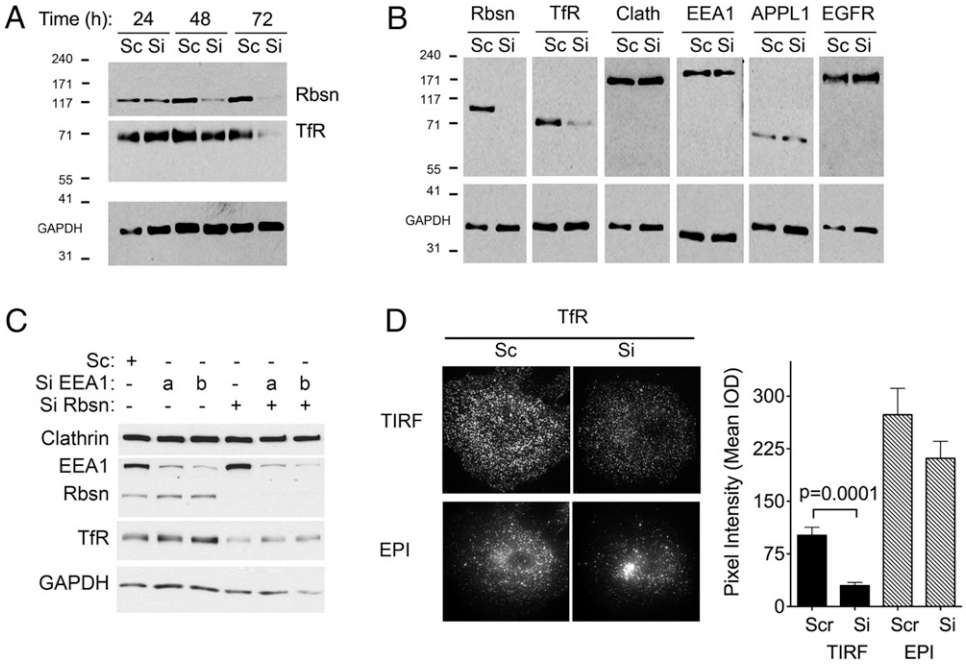

Fig. 4. Time course and effect of Rabenosyn-5 depletion on levels of endocytic proteins. Cells were transfected with scrambled (Sc) or Rabenosyn-5–directed (Si) oligonucleotides and at the time points indicated (*A*) or at 72 h (*B*) were analyzed by Western blotting for the proteins indicated. (*C*) Cells were transfected with scrambled (Sc), two different EEA1-directed (SiEEA1 a and,b), or Rabenosyn-5–directed (Si Rbsn) oligonucleotides and at 72 h were analyzed by Western blotting for the proteins indicated. (*D*) (*Left*) Representative TIRF (*Upper*) and epifluorescence (EPI) (*Lower*) images of endogenous TfR in cells transfected with scrambled (Sc) or Rabenosyn-5–directed (Si) oligonucleotides for 72 h. Epifluorescence images are autoscaled for illustration purposes to reveal the region of maximal TfR concentration. (*Right*) Quantification of the mean intensity of endogenous TfR in TIRF and EPI images.

Upper Left), with remaining receptors detected by epifluorescence in the juxtanuclear region (Fig. 4*D*, *Lower Left*). Quantification of the image intensity revealed a 75% decrease in TfR intensity in TIRF. These results reveal that the absence of Rabenosyn-5 results in a depletion of the TfR population found in the cell periphery at steady state.

To examine further how Rabenosyn-5 depletion affects TfR trafficking, we examined its internalization and recycling rates. Tf internalization was reduced markedly in cells depleted of endogenous Rabenosyn-5, and this defect could be rescued by transfection of exogenous EGFP-tagged Rabenosyn-5 (*SI Appendix*, Fig. S2). The binding of Tf to the cell surface (Fig. 5*A*) and the net amount internalized (Fig. 5*B*) were decreased significantly in cells depleted of Rabenosyn-5, consistent with the decrease in total and surface TfR levels detected by Western blotting and TIRF imaging. However, the rate of individual receptor internalization, assessed from the ratio of bound to internalized Tf (Fig. 5*C*), was not significantly different, suggesting that the lack of Rabenosyn-5 does not directly impair the very early steps of TfR recruitment into clathrin-coated vesicles. In contrast, the recycling of TfR to the plasma membrane, assessed by the release of previously internalized Tf (Fig. 5*D*), was markedly decreased by Rabenosyn-5 depletion. The major difference in recycling rate was seen in the first 15 min, suggesting that the rapid recycling pathway of the TfR (3) is affected preferentially. To compare the biochemical results to events at the single-cell level, Tf uptake and recycling were visualized by TIRF in cells expressing GFP-clathrin (Fig. 5*E*). In both control and Rabenosyn-5–depleted cells, Tf associates immediately with clathrin-enriched regions of the membrane, such that at early time points (0–30 s) virtually all the Tf signal colocalizes with clathrin (Fig. 5*E*, *Top*, yellow). Subsequently, vesicular structures appear that contain Tf but lack clathrin (Fig. 5*E*, arrows, red). At 30 s after washing these structures are likely to represent both uncoated internalizing vesicles and vesicles involved in rapid recycling of Tf; the latter gradually predominate with increasing time following removal of Tf from the medium (Fig. 5*E*, t = 240 s after washing). Recycling vesicles were greatly reduced in cells depleted of Rabenosyn-5, consistent with the finding of a slowed rapid recycling rate seen in the cell population (Fig. 5*D*).

To begin to define the mechanisms by which Rabenosyn-5 depletion leads to a decrease in TfR levels, we first examined whether its effects were exerted at the transcriptional or post-transcriptional level. Translation of the TfR is regulated through sequences in the 3′ and 5′ UTRs of its mRNA. To study the regulation of TfR levels independently of translational control, we measured the levels of TfR-EGFP expressed from a plasmid lacking the regulatory sequences present in the endogenous TfR mRNA (Fig. 6*A*). Endogenous and GFP-tagged expressed TfR levels were reduced equally in response to Rabenosyn-5 depletion, ruling out an effect of this protein on transcriptional or translational control of TfR expression. Although the majority of the TfR undergoes recycling after internalization, a larger proportion may be targeted to the lysosome for degradation in the absence of Rabenosyn-5 (33). Consistent with this possibility, exposure of cells to Bafilomycin A1, an inhibitor of acidification and lysosomal degradation, resulted in increased TfR levels (Fig. 6*B*), and this effect was more pronounced in Rabenosyn-5–depleted cells. Together these results suggest a model in which, in the absence of Rabenosyn-5, the TfR is missorted into endosomes that direct cargo toward lysosomal degradation (Fig. 6*C*).

In addition to decreased TfR levels and Tf recycling, Rabenosyn-5–depleted cells also displayed alterations in clathrin dynamics. Both the number of GFP-clathrin regions detected by TIRF (Fig. 7*A*) and their average size (Fig. 7*B*) were significantly greater in cells depleted of Rabenosyn-5. Analysis of endogenous clathrin was consistent with the results seen for GFP-clathrin, revealing an increase in the intensity of clathrin signal in the TIRF zone and the perinuclear region (Fig. 7 *C* and *D*). Because no difference in total clathrin was detected by Western blotting

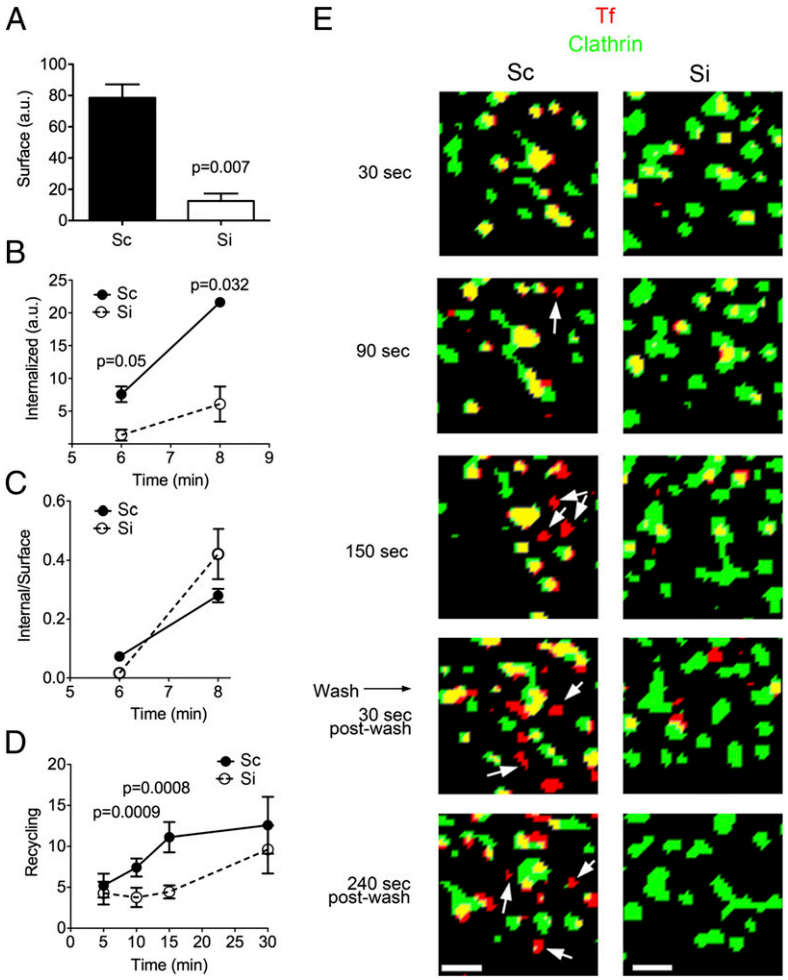

Fig. 5. Effect of Rabenosyn-5 depletion on Tf trafficking. Cells were transfected with scrambled (Sc) or Rabenosyn-5–directed (Si) oligonucleotides, and at 72 h the cell-surface binding (*A*), internalization (*B*), internalization rate (*C*), and recycling rate (*D*) were measured using HRP-labeled Tf and chemiluminescence as described in *Materials and Methods*. Plotted data are means and SEM of three experiments. Statistical significance was calculated using two-tailed Student's *t* test for each time point as indicated. (*E*) Cells were transfected with EGFP-clathrin and treated with scrambled (Sc) or Rabenosyn-5 (Si) siRNA for 72 h. Tf-DyLight-649 was added and then was removed 300 s later. Images were obtained at the indicated time points. Images were smoothed as described in Fig. 1, and binary renditions were generated to visualize all signal present. Pixel overlap is rendered in yellow. Arrows point to structures containing Tf but devoid of clathrin.

(Fig. 4*B*), and there is a significant pool of cytoplasmic unassembled clathrin in these cells (not illustrated), these results suggest that Rabenosyn-5 depletion leads to an increase in the proportion of total cellular clathrin assembled on both the plasma membrane and the trans-Golgi network. Although more work is required to understand their mechanistic basis, these findings further suggest a possible direct interaction between clathrin, or associated molecules, and Rabenosyn-5 on endosomes, possibly facilitating the delivery of cargo to the specific endosome subpopulation containing this protein.

Discussion

A large amount of evidence has demonstrated that internalization from the plasma membrane proceeds through clathrin-dependent and -independent mechanisms (4) and that variation exists within these mechanisms, whereby, for example, certain subpopulations of clathrin-coated pits may capture different receptor types preferentially (31, 34). Until recently it was thought that these diverse internalization mechanisms delivered cargo into a homogenous population of early endosomes from which sorting to different destinations occurred. However, recent genetic and imaging results have suggested that early endosomes may not be functionally homogeneous, displaying differences in composition, cargo enrichment, and motility (14–18). The findings of varied internalization mechanisms at the plasma membrane and of different endosome subpopulations raise the question of whether different internalization mechanisms are associated with distinct endosome subtypes.

To address this question, we investigated whether the TfR, internalized through clathrin-mediated endocytosis, would be delivered to a specific endosome subpopulation. This investigation required the use of a platform that could detect three fluorophores simultaneously with high temporal and spatial resolution in live cells and analytical methods to generate quantitative models from resulting complex images. By simultaneously monitoring clathrin and early endosome markers, it was possible to visualize Tf internalizing from clathrin-coated membrane structures into endosomes containing specific markers. The resulting images and kinetic models derived from quantitative analysis indicated that Tf enters endosomes containing Rabenosyn-5 almost immediately following its entry through clathrin-coated structures. By enhancing axial resolution in the TIRF zone by combining TIRF and ESL, it was found that Rabenosyn-5–enriched endosomes reside closest to clathrin-enriched structures at the plasma membrane, providing a topological framework for delivery of Tf into this specific endosome population.

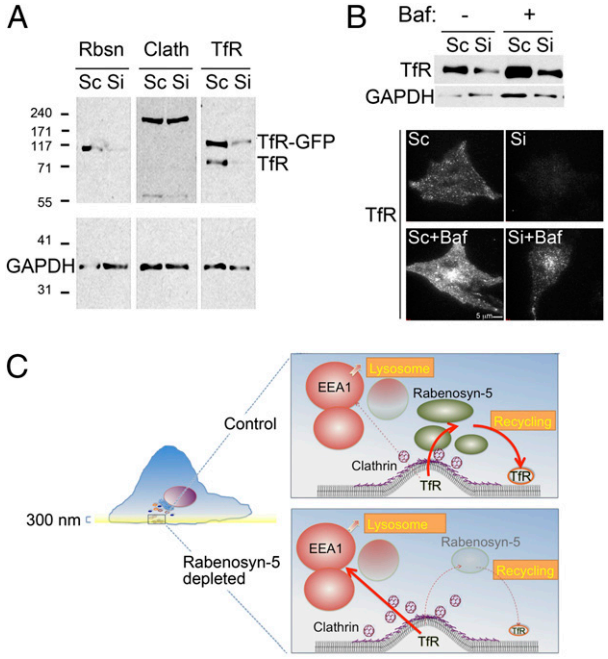

Fig. 6. Mechanism of TfR loss in response to Rabenosyn-5 depletion. (*A*) Western blotting of TfR in cells transfected with TfR-GFP and treated with scrambled (Sc) or Rabenosyn-5 (Si) siRNA for 72 h after transfection. GAPDH is used as a loading control. (*B*) Cells were transfected with scrambled (Sc) or Rabenosyn-5–directed (Si) oligonucleotides and 48 h were left untreated or were treated with 100 nM Bafilomycin A1 (Baf). After 24 h lysates were harvested and analyzed by Western blotting and immunofluorescence for the TfR. (*C*) In this model, TfR is internalized into endosomes marked by Rabenosyn-5, which are juxtaposed to clathrin-coated plasma membrane regions; from these endosomes TfR is recycled rapidly to the plasma membrane. A small fraction of TfR may be directed into EEA1-enriched endosomes, which are destined for lysosomal degradation. In the absence of Rabenosyn-5, clathrin-coated structures accumulate, and their cargo enters lysosome-directed pathways, resulting in low recycling rates.

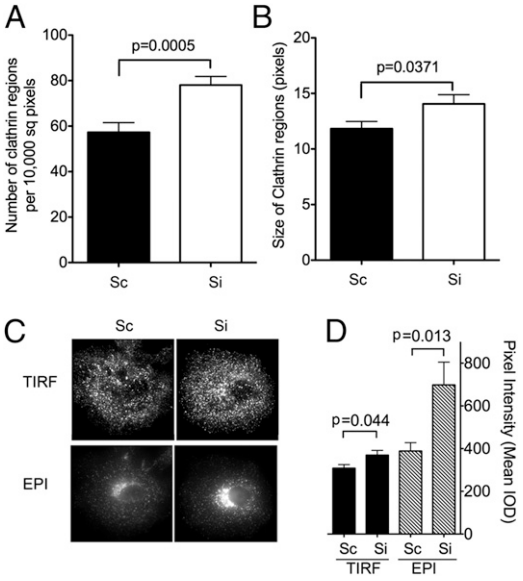

Fig. 7. Effect of Rabenosyn-5 depletion on clathrin distribution. Cells were transfected with EGFP-clathrin and treated with scrambled (Sc) or Rabenosyn-5 (Si) siRNA for 72 h. The number (*A*) and size (*B*) of clathrin regions in the TIRF zone was determined from binary renditions of smoothed images such as those depicted in Fig. 5*E*. Results are the means and SEM of regions from 8–10 cells. (*C*) Representative TIRF (*Upper*) and epifluorescence (*Lower*) images of endogenous clathrin in cells transfected with scrambled (Sc) or Rabenosyn-5–directed (Si) oligonucleotides for 72 h. (*D*) Quantification of the mean intensity of endogenous clathrin in TIRF and epifluorescence (EPI) images. Results are the means and SEM of 8–10 cells. Statistical significance was calculated using two-tailed Student's *t* test.

The results discussed above led us to test the hypothesis that Rabenosyn-5 might be functionally involved in the movement of TfR from clathrin-coated structures into endosomes. Biochemical and morphological analysis revealed impairment in rapid TfR recycling following internalization and a marked increase in TfR degradation. In conjunction, the dynamics of clathrin at the plasma membrane appear altered, with the size and number of clathrin-enriched regions being increased. Clathrin-enriched regions at the plasma membrane are larger than individual clathrin-coated pits and vesicles and are likely to represent areas of enhanced formation of these structures (20, 31, 32). Thus, an increase in their size and number may reflect a delay in the movement of clathrin-coated vesicles away from the plasma membrane or a delay in their uncoating and fusion with endosomes (Fig. 6*C*). These results are consistent with previous findings of impaired formation of early endosomes in *Drosophila* and *Caenorhabditis elegans* lacking Rabenosyn-5 (35, 36) and with previous results in mammalian cells indicating a role for this protein in receptor recycling (20, 26, 37). Moreover, a direct role of Rabenosyn-5 in clathrin-mediated internalization may explain the mechanism by which dominant negative mutants of Rab5, which interacts with Rabenosyn-5 (38), impair Tf uptake (39).

Beyond identifying Rabenosyn-5 as an important regulator of TfR entry into the endosomal pathway, the data shown here suggest that sorting in general may occur through delivery of cargo into specific endosome subpopulations that maintain a defined topological organization relative to sites of endocytosis. Results by others also are consistent with the concept that diverse endocytic mechanisms are associated with specific endosomal subtypes. For example, work by Zoncu et al. (18) indicates that EGFR is internalized via macropinosomes that rapidly acquire APPL1 and subsequently acquire WD repeat and FYVE domain-containing protein 2 (WDFY2) and EEA1. We (15) and others (40) also have observed that EGF is internalized from the plasma membrane into EEA1-containing endosomes and have found relatively low colocalization of internalizing Tf with EEA1 (15, 19, 41). Moreover, knockdown of EEA1 leads to a detectable increase in TfR levels (Fig. 4) and to an impairment of EGFR degradation (15), in stark contrast to the effect of Rabenosyn-5 knockdown in decreasing TfR levels. These results support a model in which EEA1 and Rabenosyn-5 have fundamentally different roles in endosomal traffic: Endosomes containing EEA1 appear to capture cargo destined to lysosomes, whereas endosomes containing Rabenosyn-5 capture cargo destined for recycling (Fig. 6*C*).

Despite these different functions, many endosomes containing both Rabenosyn-5 and EEA1 are found deeper within the cell (42), but how these endosomes arise is not clear. In one possible model, endosomes formed from larger portions of the membrane, such as EGF-containing macropinosomes that acquire EEA1 (18, 43), also may acquire Rabenosyn-5 in conjunction with endosomal clathrin for the purpose of fully retrieving cargo that is not destined for the lysosomal pathway, as has been shown to occur for E-cadherin (44). Alternatively, EEA1 may associate with Rabenosyn-5–enriched endosomes to retrieve cargo destined for degradation. This association is likely to vary with the levels of phosphatidylinositol 3-phosphate and Rab5 unoccupied by Rabenosyn-5. Thus, cargoes such as EGF, which increase the activity of PI3 kinases and activate Rab5 (45), would be expected to promote binding of EEA1 to Rabenosyn-5–containing endosomes. Activation of Rab5 also would be expected to result in enhanced EEA1 binding and

more extensive colocalization of Rabenosyn-5 and EEA1 on the same endosomal surface, as indeed is observed in cells overexpressing wild-type or persistently active Rab5 (42).

In summary, the visualization of the initial steps of endocytosis using a multimodal imaging platform that improves axial resolution in TIRF and the use of analysis protocols that generate quantitative models from complex imaging data have identified Rabenosyn-5 as a key element in clathrin-mediated endocytosis and the initial node of Tf sorting. Further experiments with additional ligands and endosomal components will allow generation of quantitative, testable models for the molecular mechanisms underlying receptor internalization into the endocytic pathway.

Materials and Methods

Cell Culture and Transfection. COS-7 cells were maintained in DMEM (Invitrogen) supplemented with 100 U/mL penicillin streptomycin (Invitrogen), 0.1 mg/mL Normocin (InvivoGen), and 10% FBS (Atlanta Biologicals) at 37 °C, 5% CO_2. Cells were plated at a density of 1×10^5 cells per well in a six-well cell-culture plate and grown for 24 h. These cells were transfected with 1 μg DNA using calcium phosphate, grown for 24 h and then re-plated on glass coverslips (25-mm circles, #1.5; Thomas Scientific), and grown for an additional 24 h. Live imaging was done in KRH buffer (125 M NaCl, 5 mM KCl, 1.3 mM CaCl2, 1.2 mM $MgSO_4$, 25 mM Hepes, 2.5% BSA, and 2 mM sodium pyruvate), pH 7.4.

RNAi. Rabenosyn-5 and EEA1 RNAi duplexes with a sense sequence of 5′-UUUGAUGUCACUGCCAACCAAAGAA-3′ and 5′-AGGACCAAAAGAUCCAGAACCUUGA-3′, respectively, were designed and synthesized by RXi Pharmaceuticals. A second oligonucleotide to EEA1, with the sense sequence 5′-AACUUGCUACUGAAAUUGCAGUU-3′ (designated "a" in Fig. 6*D*) was obtained from Dharmacon. One day before transfection cells were plated in antibiotic-free medium in a six-well cell-culture plate at a density of 1×10^5 cells per well. Cells were transfected using 5 μL of Lipofectamine RNAiMAX (Invitrogen) according to the manufacturer's instructions with a final concentration of 10 nM siRNA.

Reagents. Polyclonal EEA1 antibody was produced in chickens by injecting N-terminal 6-His–tagged fusion protein of human EEA1 residues 32–218. Polyclonal clathrin antibody was produced in rabbits by injecting the last 15 amino acids of the clathrin heavy chain. Polyclonal Rabenosyn-5 antibody was produced in rabbits by injecting residues 137–784 of human Rabenosyn-5. Additional antibodies were obtained as follows: APPL1 and GAPDH from Cell Signaling Technologies; TfR from Invitrogen, and EGFR from Millipore. Unconjugated, DyLight-649– and DyLight-488–conjugated human Tf were obtained from Jackson Immunochemicals.

Plasmids. TagRFP-T in pcDNA3 and TagRFP-T-clathrin were gifts from Roger Y. Tsien (University of California at San Diego, La Jolla, CA) and Michael W. Davidson (Florida State University, Tallahassee, FL), respectively. The TagRFP-T expression vector was constructed as described (46). GFP-clathrin was a gift from J. H. Keen (Thomas Jefferson University, Philadelphia, PA). The cDNA clone 40034008 for human Rabenosyn-5 was obtained from American Tissue Culture Collection and was cloned in frame with EGFP or TagRFP-T at the N terminus of the protein using standard techniques. GFP-EEA1, from which TagRFP-T-EEA1 was subcloned, was described previously (47). APPL1 (48) was cloned in frame with EGFP and TagRFP-T at the N terminus of the protein using standard techniques. Human TfR in plasmid cDNA was a gift from Tim McGraw (Weill-Cornell Medical College, New York, NY). Human TfR cDNA was subcloned in frame with EGFP in the Clontech pEGFP-N1 vector at the XhoI and BamHI restriction sites.

TESM Optical System. A custom-built microscope system, TESM, simultaneously combines TIRF and wide-field epifluorescence modes and incorporates structured illumination in the epi mode for fast optical sectioning and enhanced spatial resolution. Further details are given in the *SI Appendix*.

TESM Imaging Hardware and Software. The TESM acquisition system is described in the *SI Appendix*.

TIRF Time Series Imaging. The TIRF time series protocol used three lasers emitting at 491 and 561 nm, with 525/50- and 590/50-nm emission filters, respectively, and at 660 nm, with >690 nm emission. By using four-color (blue, green, orange-red, far-red) 0.2-μm TetraSpeck microspheres (Invitrogen), it was determined that the focus (and magnification) of the green (525 nm) and red (590 nm) emission were identical, whereas the far-red (690 nm) focus was shifted by 500 nm. Correspondingly, the focus of the microscope was shifted by this amount using a PIFOC objective scanner (Physik Instruments) when acquiring the far-red images.

TESM 3D Imaging. The same lasers and emission filters were used in the TESM imaging protocol as in TIRF alone. Typically, each set of images contained one TIRF image followed by three structured light images. The grating was moved by one-third of a period (~2 ms) between each image. The period of the grating was 500 line-pairs/in; with the 60× objective, the first-order period at the specimen was measured to be 0.456 microns, and no higher orders were observable. The focus was adjusted by 0.1 microns between every set of images for a total range of 10 microns.

TIRF Image Analysis. For quantitative image analysis, TIRF time-series images first were smoothed by performing a temporal running average of three time points to reduce noise with a negligible effect on data. Next, the background fluorescence for each image was calculated as the mean intensity in a region of interest (typically 21 × 21 pixels) outside the cell and was subtracted from all pixels.

Segmentation of vesicles from background. To generate images in which vesicles or other fluorescence structures can be analyzed without interference from diffuse fluorescence, images then were convolved with a DOG filter consisting of (*i*) a small 2D Gaussian spot with a unit area (σ = 150 nm) that acted as a vesicle-matched detector (i.e., an approximation to a near-diffraction limited spot) and (*ii*) a larger, inverted 2D Gaussian spot (σ = 300 nm) with negative unit area that estimated and subtracted the local background. The Gaussian smoothed images were thresholded visually (global threshold) to select for pixels belonging to objects (e.g., vesicles) and to eliminate areas devoid of signal but containing noise.

Colocalization. For colocalization analysis, image sets dual labeled or triple labeled with Tf-DyLight 649 were processed as above. For each label, its globally thresholded image was used to generate a binary image by setting the intensity of all positive-value pixels to one and all other pixels to zero. Colocalization was determined by two-way or three-way binary image overlap among the labels. Colocalization values are reported as the percent of pixels that are colocalized with a given label. Given a pair of 2D binary images of labels "A" and "B," the colocalization of B with A at time *t* is

$$100 \cdot \sum_x \sum_y [A(x,y,t) \cdot B(x,y,t)] / \sum_x \sum_y B(x,y,t)$$

Images of two-way and three-way colocalization are displayed using the running-averaged, background-subtracted images (colored as green and red or as green, red, and blue), with the colocalized pixels (defined above) shown as white, as indicated by the accompanying color wheels (Figs. 1 and 3) (49).

Tf trafficking. To analyze the trafficking of Tf, the thresholded-DOG time-series image of an endocytic marker (clathrin, Rabenosyn-5, APPL, EEA1) was analyzed to identify individual objects (spots, vesicles) and their central (x,y,t) positions in every time point by finding all 2D intensity maxima (pixels brighter than their eight neighbors) and thresholding the maxima to eliminate spurious peaks. The average local fluorescence within a 5 × 5 pixel region centered at each (x,y,t) position was obtained in both the running-averaged, background-subtracted endocytic marker image and the corresponding Tf image. From this value, the average fluorescence of a one-pixel-wide frame surrounding the 5 × 5 pixel region was subtracted (e.g., Fig. 1*B*). The fluorescence ratio of Tf to endocytic marker was calculated for each object position, and the mean ratio and SE for each time point was calculated (typically there were hundreds of objects in each time point) and plotted (e.g., Figs. 1*C* and 3*B*). The fluorescence ratio was used as an estimate of the (relative) Tf concentration associated with each object (both signals should be in roughly some proportion to the amount of surface membrane) while also correcting for the exponential decrease in fluorescence brightness with increasing depth in TIRF. Additionally, the kinetics of trafficking of Tf through clathrin, Rabenosyn-5, and APPL1 were modeled, and the models were fit to the ratio time-course data to determine rates of entry/filling and exiting/emptying of Tf for each endocytic marker. Details of the kinetic models and fitting are given in the *SI Appendix* material.

TESM 3D Image Analysis. Optical sections images of epifluorescence were produced from the structured illumination data sets according to the method of Tony Wilson (22). Briefly, at each focal position and for each emission wavelength, a single optical section image, I, was computed from a triplet of images acquired sequentially with the illumination grating shifted by one-third period each time ($I_{0/3}$, $I_{1/3}$ and $I_{2/3}$) as

$$I = \left[\left(I_{0/3} - I_{1/3}\right)^2 + \left(I_{1/3} - I_{2/3}\right)^2 + \left(i_{2/3} - I_{0/3}\right)^2 \right]^{1/2}$$

Colocalization. Optical section images of endogenous proteins (antibody-labeled and fixed) were convolved with a 2D DOG filter with the positive unit area Gaussian ρ = 75 nm and the negative unit area Gaussian ρ = 150 nm. Selected focal positions of the DOG images were used to generate binary images as described above. Colocalization between proteins was determined by two- or three-way binary image overlap.

TESM Z-position maps. False-colored maps of the axial (*z*) position of fluorescence were created from the combination of TIRF and optical section images. TIRF images confound "intrinsic" fluorescence brightness with axial position. If the actual brightness is known, then the axial position can be recovered. The epifluorescence- structured illumination optical section images were used as indicators of actual in-focus fluorescence brightness. Briefly, the 3D TIRF images of both 491 and 561 nm illuminations were inspected to determine a single, nearest to the coverslip (in 100-nm steps) plane of best focus, z0, of all of the visible structures. The TIRF and the optical section image stacks at both wavelengths then were segmented to span from z0–2 to z0+4, or 700 nm of depth, and a single "extended focus" image of both TIRF and epifluorescence was made by maximum intensity projection of these seven planes, yielding a set of four images ($^{491}I_{TIRF}$, $^{491}I_{epi}$, $^{561}I_{TIRF}$, and $^{561}I_{epi}$). These images were thresholded to excluded areas devoid of signal.

Because there is a microscope system dependent and illumination wavelength (λ) dependent difference in excitation efficiency between the TIRF and epi-illumination paths (the emission path is the same), there is a scale factor $^{\lambda}K$ relating the intensity of the TIRF image $^{\lambda}I_{TIRF}$ to the epi image $^{\lambda}I_{epi}$. If the the e^{-1} penetration distance d of the TIRF evanescent field is known, then image *Z* of axial positions of fluorescent sources in the field can be calculated as

$$Z = -^{\lambda}d \cdot \ln\left[{}^{\lambda}K \cdot {}^{\lambda}I_{TIRF} / {}^{\lambda}I_{epi}\right]$$

$$Z = -^{\lambda}d \cdot \ln\left[{}^{\lambda}I_{TIRF} / {}^{\lambda}I_{epi}\right] + \left(-^{\lambda}d \cdot \ln\left[{}^{\lambda}K\right]\right)$$

$$Z = -^{\lambda}d \cdot \ln\left[{}^{\lambda}I_{TIRF} / {}^{\lambda}I_{epi}\right] + {}^{\lambda}z_0$$

The value of z_0 depends on *d* and *K* and is constant as long as the microscope set up is constant. There is an axial apparent offset between the wavelengths Δz = ($^{491}z_0$ – $^{561}z_0$). This offset was determined empirically using dual-color microspheres and is described in *SI Appendix*, Fig. S1.

Biochemical Measurement of Tf Trafficking. Cells were treated with scrambled (control) or Rabenosyn-5 siRNA as described. At 48 h knockdown cells were replated on black 96-well plates at a density of 1.5×10^4 cells per well and cultured for an additional 24 h at 37 °C, 5% CO_2. Serum Tf was removed by incubation in DMEM (Invitrogen) supplemented with 1% ovalbumin (Sigma) for 1 h at 37 °C 5%, CO_2. To determine the number of TfR on the cell surface, cells were incubated on ice with DMEM supplemented with 1% ovalbumin containing 10 μg/mL peroxidase-conjugated human Tf (Tf-HRP) (Jackson ImmunoResearch). After 2 h cells were washed, and peroxidase activity was detected using SuperSignal ELISA Pico Chemiluminescent Substrate (Pierce) using a Tecan Safire2. To measure internalization rates, cells were incubated at 37 °C with DMEM containing 1% ovalbumin and 10 μg/mL Tf-HRP. At the times indicated in each figure cells were placed on ice and washed three times with chilled PBS supplemented with 5% ovalbumin and three times with neutral pH buffer supplemented with 1% ovalbumin. Then half the wells were exposed to chilled pH 2.0 buffer (500 mM NaCl, 0.2 N glacial acetic acid) for 5 min at 4 °C. Cells were washed twice with neutral pH buffer and once with PBS, and chemiluminescence was detected as described above. Internalized Tf was defined as the difference in signal between acid-washed (internalized) and non–acid-washed (total) wells. To measure recycling rates, cells were incubated at 37 °C 5%, CO_2 for 2 h in DMEM supplemented with 1% ovalbumin containing 10 μg/mL Tf-HRP. Cells were washed once with PBS supplemented with 5% ovalbumin and incubated in pH 5.0 buffer (150 mM NaCl, 50 mM MES) at room temperature for 2 min. Cells were washed three times with prewarmed efflux medium (DMEM supplemented with 100 μM desferoxamine and 10 μg/mL human Tf). At the times indicated, medium was removed, and chemiluminescence in the medium was detected as described above. In each experiment values obtained in the presence of a 200-fold excess of unconjugated human Tf were subtracted to obtain specific signal. Means and SEM are for three independent experiments performed in quadruplicate.

ACKNOWLEDGMENTS. Core services were supported by University of Massachusetts Diabetes Endocrinology Research Center Grant DK32520. This work was supported by National Institutes of Health Grants PO1 DK60564 and DK60837.

1. Mellman I (1995) Molecular sorting of membrane proteins in polarized and nonpolarized cells. *Cold Spring Harb Symp Quant Biol* 60:745–752.
2. Gruenberg J, Maxfield FR (1995) Membrane transport in the endocytic pathway. *Curr Opin Cell Biol* 7:552–563.
3. Maxfield FR, McGraw TE (2004) Endocytic recycling. *Nat Rev Mol Cell Biol* 5:121–132.
4. Doherty GJ, McMahon HT (2009) Mechanisms of endocytosis. *Annu Rev Biochem* 78: 857–902.
5. Li L, Guan KL (2009) Amino acid signaling to TOR activation: Vam6 functioning as a Gtr1 GEF. *Mol Cell* 35:543–545.
6. Sancak Y, et al. (2010) Ragulator-Rag complex targets mTORC1 to the lysosomal surface and is necessary for its activation by amino acids. *Cell* 141:290–303.
7. Siomi H, Siomi MC (2009) RISC hitches onto endosome trafficking. *Nat Cell Biol* 11: 1049–1051.
8. Lee YS, et al. (2009) Silencing by small RNAs is linked to endosomal trafficking. *Nat Cell Biol* 11:1150–1156.
9. Gibbings DJ, Ciaudo C, Erhardt M, Voinnet O (2009) Multivesicular bodies associate with components of miRNA effector complexes and modulate miRNA activity. *Nat Cell Biol* 11:1143–1149.
10. Jovic M, Sharma M, Rahajeng J, Caplan S (2010) The early endosome: A busy sorting station for proteins at the crossroads. *Histol Histopathol* 25:99–112.
11. Gruenberg J (2003) Lipids in endocytic membrane transport and sorting. *Curr Opin Cell Biol* 15:382–388.
12. Bonifacino JS, Traub LM (2003) Signals for sorting of transmembrane proteins to endosomes and lysosomes. *Annu Rev Biochem* 72:395–447.
13. Mellman I (1996) Endocytosis and molecular sorting. *Annu Rev Cell Dev Biol* 12: 575–625.
14. Collinet C, et al. (2010) Systems survey of endocytosis by multiparametric image analysis. *Nature* 464:243–249.
15. Leonard D, et al. (2008) Sorting of EGF and transferrin at the plasma membrane and by cargo-specific signaling to EEA1-enriched endosomes. *J Cell Sci* 121:3445–3458.
16. Hayakawa A, et al. (2006) The WD40 and FYVE domain containing protein 2 defines a class of early endosomes necessary for endocytosis. *Proc Natl Acad Sci USA* 103: 11928–11933.
17. Lakadamyali M, Rust MJ, Zhuang X (2006) Ligands for clathrin-mediated endocytosis are differentially sorted into distinct populations of early endosomes. *Cell* 124: 997–1009.
18. Zoncu R, et al. (2009) A phosphoinositide switch controls the maturation and signaling properties of APPL endosomes. *Cell* 136:1110–1121.
19. Sheff D, Pelletier L, O'Connell CB, Warren G, Mellman I (2002) Transferrin receptor recycling in the absence of perinuclear recycling endosomes. *J Cell Biol* 156:797–804.
20. Traub LM (2011) Regarding the amazing choreography of clathrin coats. *PLoS Biol* 9: e1001037.
21. Karadaglić D, Wilson T (2008) Image formation in structured illumination wide-field fluorescence microscopy. *Micron* 39:808–818.
22. Neil MA, Juskaitis R, Wilson T (1997) Method of obtaining optical sectioning by using structured light in a conventional microscope. *Opt Lett* 22:1905–1907.
23. Dumas JJ, et al. (2001) Multivalent endosome targeting by homodimeric EEA1. *Mol Cell* 8:947–958.
24. Christoforidis S, McBride HM, Burgoyne RD, Zerial M (1999) The Rab5 effector EEA1 is a core component of endosome docking. *Nature* 397:621–625.
25. Miaczynska M, et al. (2004) APPL proteins link Rab5 to nuclear signal transduction via an endosomal compartment. *Cell* 116:445–456.
26. Nielsen E, et al. (2000) Rabenosyn-5, a novel Rab5 effector, is complexed with hVPS45 and recruited to endosomes through a FYVE finger domain. *J Cell Biol* 151:601–612.
27. Lindmo K, Stenmark H (2006) Regulation of membrane traffic by phosphoinositide 3-kinases. *J Cell Sci* 119:605–614.
28. Shin HW, et al. (2005) An enzymatic cascade of Rab5 effectors regulates phosphoinositide turnover in the endocytic pathway. *J Cell Biol* 170:607–618.
29. Corvera S, D'Arrigo A, Stenmark H (1999) Phosphoinositides in membrane traffic. *Curr Opin Cell Biol* 11:460–465.
30. Merrifield CJ, Perrais D, Zenisek D (2005) Coupling between clathrin-coated-pit invagination, cortactin recruitment, and membrane scission observed in live cells. *Cell* 121:593–606.
31. Traub LM (2009) Clathrin couture: Fashioning distinctive membrane coats at the cell surface. *PLoS Biol* 7:e1000192.
32. Bellve KD, et al. (2006) Plasma membrane domains specialized for clathrin-mediated endocytosis in primary cells. *J Biol Chem* 281:16139–16146.
33. Zaliauskiene L, et al. (2000) Down-regulation of cell surface receptors is modulated by polar residues within the transmembrane domain. *Mol Biol Cell* 11:2643–2655.
34. Conner SD, Schmid SL (2003) Differential requirements for AP-2 in clathrin-mediated endocytosis. *J Cell Biol* 162:773–779.

35. Morrison HA, et al. (2008) Regulation of early endosomal entry by the Drosophila tumor suppressors Rabenosyn and Vps45. *Mol Biol Cell* 19:4167–4176.
36. Gengyo-Ando K, et al. (2007) The SM protein VPS-45 is required for RAB-5-dependent endocytic transport in Caenorhabditis elegans. *EMBO Rep* 8:152–157.
37. Naslavsky N, Boehm M, Backlund PS, Jr., Caplan S (2004) Rabenosyn-5 and EHD1 interact and sequentially regulate protein recycling to the plasma membrane. *Mol Biol Cell* 15:2410–2422.
38. Eathiraj S, Pan X, Ritacco C, Lambright DG (2005) Structural basis of family-wide Rab GTPase recognition by rabenosyn-5. *Nature* 436:415–419.
39. Bucci C, et al. (1992) The small GTPase rab5 functions as a regulatory factor in the early endocytic pathway. *Cell* 70:715–728.
40. Yoon HY, Lee JS, Randazzo PA (2008) ARAP1 regulates endocytosis of EGFR. *Traffic* 9: 2236–2252.
41. Wegner CS, et al. (2010) Ultrastructural characterization of giant endosomes induced by GTPase-deficient Rab5. *Histochem Cell Biol* 133:41–55.
42. de Renzis S, Sönnichsen B, Zerial M (2002) Divalent Rab effectors regulate the sub-compartmental organization and sorting of early endosomes. *Nat Cell Biol* 4:124–133.
43. Hamasaki M, Araki N, Hatae T (2004) Association of early endosomal autoantigen 1 with macropinocytosis in EGF-stimulated A431 cells. *Anat Rec A Discov Mol Cell Evol Biol* 277:298–306.
44. Bryant DM, et al. (2007) EGF induces macropinocytosis and SNX1-modulated recycling of E-cadherin. *J Cell Sci* 120:1818–1828.
45. Barbieri MA, et al. (2000) Epidermal growth factor and membrane trafficking. EGF receptor activation of endocytosis requires Rab5a. *J Cell Biol* 151:539–550.
46. Shaner NC, et al. (2008) Improving the photostability of bright monomeric orange and red fluorescent proteins. *Nat Methods* 5:545–551.
47. Lawe DC, et al. (2002) Sequential roles for phosphatidylinositol 3-phosphate and Rab5 in tethering and fusion of early endosomes via their interaction with EEA1. *J Biol Chem* 277:8611–8617.
48. Saito T, Jones CC, Huang S, Czech MP, Pilch PF (2007) The interaction of Akt with APPL1 is required for insulin-stimulated Glut4 translocation. *J Biol Chem* 282: 32280–32287.
49. Lifshitz LM, Collins JA, Moore ED, Gauch J (1994) Computer vision and graphics in fluorescence microscopy. *Proceedings of the IEEE Workshop on Biomedical Image Analysis*, Seattle, WA, June 24–25, 1994. (IEEE Computer Society, Los Alamitos, CA).